Nano Research

Open Access

Research Article

Mild alkaline-assisted silver deposition on PLA fibers for ultra-high and sustainable electromagnetic interference shielding

Jia-Le Zhang[1], Sheng Yong[1], Jie Li[2] ✉, Yue-Yi Wang[2], Ling Xu[2], Gan-Ji Zhong[1], Ding-Xiang Yan[1,2] ✉, and Zhong-Ming Li[1,3]

[1] College of Polymer Science and Engineering, State Key Laboratory of Advanced Polymer Materials, Sichuan University, Chengdu 610065, China
[2] School of Aeronautics and Astronautics, Robotic Satellite Key Laboratory of Sichuan Province, Key Laboratory of Advanced Spatial Mechanism and Intelligent Spacecraft, Ministry of Education, Sichuan University, Chengdu 610065, China
[3] Institute of Cardiovascular Surgery, West China Hospital, Sichuan University, Chengdu 610041, China

Cite this article: *Nano Research*, **2026**, *19*, 94908333. https://doi.org/10.26599/NR.2026.94908333

ABSTRACT: The proliferation of electromagnetic spectrum applications and increasing integration density of electronic devices have intensified electromagnetic pollution, driving demand for advanced electromagnetic interference (EMI) shielding materials. While conductive polymer composites present promising alternatives to traditional metals, attaining both exceptional EMI shielding performance and environmental sustainability remains challenging. Here, we adopt controlled mild alkaline hydrolysis to precisely engineer the surface roughness and hydrophilicity of polylactic acid (PLA) fibers, generating optimal substrates for subsequent electroless silver (Ag) deposition. The resulting Ag/PLA conductive fibers are structured into flexible films through vacuum filtration and hot-pressing. These films demonstrate remarkable electrical conductivity of 102,270 S/m, attributed to the continuous Ag coating and three-dimensional fibrous conductive network. Despite a thickness of merely 66 μm, the Ag/PLA films exhibit an ultra-high EMI shielding effectiveness (EMI SE) of 101.0 dB and a specific shielding effectiveness of 9749.4 dB·cm²/g. Notably, the films maintain military-grade EMI shielding performance (> 90 dB) after thermal cycling across a ~ 300 °C temperature range and 5000 bending cycles, confirming superior durability and mechanical flexibility. By synergistically coupling biodegradable PLA with recoverable Ag, this work simultaneously achieves outstanding EMI shielding performance and environmental sustainability, providing valuable insights for developing next-generation green EMI protection materials.

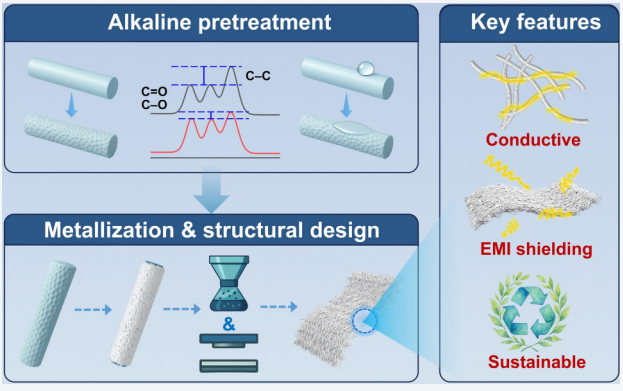

KEYWORDS: electromagnetic interference (EMI) shielding, polylactic acid (PLA), surface functionalization, electroless silver plating

1 Introduction

Electromagnetic interference (EMI) presents a critical challenge in modern electronics, threatening both human health and device reliability [1–3]. The development of high-performance EMI shielding materials has thus become imperative [4, 5]. Emerging applications in wearable and flexible electronics demand materials that integrate lightweight construction, minimal thickness, and superior EMI shielding effectiveness (EMI SE) [6–8]. While conventional bulk metals suffer from excessive weight, inherent brittleness, and corrosion susceptibility, conductive polymer composites (CPCs) offer compelling advantages through their low density, tailorable properties, and excellent processability [9–11].

Incorporating conductive fillers into flexible polymer matrices remains the predominant strategy for fabricating CPCs [12–14]. According to percolation theory and Schelkunoff theory, achieving effective EMI shielding requires either high filler loadings or efficient conductive networks [15, 16]. For example, Zhao et al.

Received: September 29, 2025; **Revised:** November 11, 2025
Accepted: December 11, 2025

✉Address correspondence to Jie Li, jieli0619@scu.edu.cn; Ding-Xiang Yan, yandingxiang@scu.edu.cn

developed carbon nanotube (CNT)/polyurethane composites that exhibited an EMI SE of 59.74 dB at a high CNT loading of 80 wt.% [17]. However, such elevated filler concentrations inevitably compromise the mechanical flexibility of the resulting composites, limiting their practical applications [18–20]. Surface deposition of continuous conductive coatings on flexible polymer substrates offers a promising alternative, delivering outstanding EMI shielding performance while largely preserving the intrinsic mechanical properties of the substrates [21–23]. Among various deposition techniques, electroless plating provides distinct advantages, including uniform coverage of complex geometries and straightforward processing procedures [24–26]. Silver (Ag), with its unparalleled electrical conductivity (6.3×10^7 S/m) and remarkable chemical stability, represents an ideal coating material for achieving ultra-high EMI SE (> 90 dB) [27–29]. Li et al. fabricated continuous Ag nanoparticle (AgNP) coatings on commercial nylon mesh surfaces via electroless plating, demonstrating notable EMI shielding performance (91.6 dB) with sustained mechanical flexibility (80 dB retention after 5000 bending cycles) [30]. Nevertheless, the surface hydrophobicity and chemical inertness of most polymer substrates present significant challenges for direct Ag deposition and robust interfacial adhesion, thereby necessitating appropriate surface pretreatment strategies [31–33].

Concentrated strong acid/base etching (> 2 M) constitutes the most widely adopted surface pretreatment method for enhancing polymer surface roughness and facilitating electroless Ag plating [34, 35]. For instance, Tang et al. successfully deposited AgNPs on polyimide (PI) nonwoven fabrics following treatment with 2.8 M sodium hydroxide solution, attaining an EMI SE of 67.5 dB at 60 μm thickness [36]. Although novel approaches such as plasma treatment and coupling agent modification have been explored, their practical implementation remains limited by poor stability and operational complexity [37–39]. Consequently, developing mild yet effective surface pretreatment strategies for polymer surfaces emerges as an urgent challenge.

Polylactic acid (PLA), a representative biopolymer, has been extensively investigated for its favorable biocompatibility and mechanical properties comparable to those of conventional plastics [40–42]. The unique chemical structure of PLA enables controllable surface modification via hydrolysis under mild alkaline conditions [43, 44]. Yang et al. demonstrated this approach by treating PLA films with 0.25 M NaOH/ethanol solution at room temperature for 52 h, resulting in a dramatic reduction in water contact angle from 78.0° to 12.6° [45]. This treatment substantially enhanced surface hydrophilicity and roughness while avoiding severe bulk degradation. Moreover, PLA completely breaks down within days to months under enzymatic or composting conditions [46, 47]. The synergistic combination of inherent biodegradability and tunable surface functionalization positions PLA as an ideal substrate for developing high-performance and sustainable EMI shielding materials.

In this work, we employed a mild alkaline pretreatment strategy that exploits the hydrolytic susceptibility of PLA to achieve effective surface hydrophilization and roughening of PLA fibers. Ag-coated PLA fibers (Ag/PLA fibers) were prepared through electroless plating, then processed via vacuum filtration and hot pressing to fabricate flexible Ag/PLA composite films. The continuous and dense AgNP layer on the fiber surface, coupled with the three-dimensional interwoven fibrous network architecture, yielded exceptional EMI SE of 101.0 dB and impressive specific shielding effectiveness (SSE/*t*) of 9749.4 dB·cm²/g. The composite films exhibited excellent environmental stability and mechanical flexibility, maintaining superior EMI SE (> 90 dB) under extreme temperatures, corrosive conditions, and mechanical deformation. By integrating biodegradable PLA with highly conductive Ag, this work demonstrates a synergistic approach that combines high performance with environmental sustainability, providing a scalable pathway toward next-generation green EMI shielding materials.

2 Experimental

2.1 Materials

PLA fibers, with an average linear density of 1.7 dtex and a length of 5 mm, were supplied by Advansa GmbH (Germany). All other chemical reagents were analytical grade, purchased from Chengdu Kelong Chemical Co., Ltd. (China), and used as received. These reagents included sodium hydroxide (NaOH), methanol (MeOH), ethanol (EtOH), hydrochloric acid (HCl), stannous chloride dihydrate ($SnCl_2{\cdot}2H_2O$), silver nitrate ($AgNO_3$), ammonia solution ($NH_3{\cdot}H_2O$), and anhydrous glucose ($C_6H_{12}O_6$). Deionized water was produced by an ultrapure water system.

2.2 Preparation of Ag/PLA films

To enhance the hydrophilicity and surface roughness of PLA fibers, an alkaline pretreatment was performed. Specifically, the PLA fibers were immersed in a MeOH/water solution (2:1 v/v) containing 0.025 M NaOH and stirred continuously at 400 rpm for various durations. After treatment, the fibers were collected by vacuum filtration, rinsed thoroughly with deionized water, and dried at 60 °C for 24 h.

For electroless Ag plating, the alkali-treated PLA fibers were first sensitized in an acidified $SnCl_2$ solution (10 g/L) for 30 min. Subsequently, the sensitized fibers were immersed in a fresh silver-ammonia complex solution, which was prepared by adding $NH_3{\cdot}H_2O$ dropwise to an $AgNO_3$ solution (4 g/L) until complete dissolution of the initially formed precipitate. Excess glucose solution was then introduced as the reducing agent to initiate AgNP deposition on the fiber surfaces. After 3 h reaction at room temperature, silver-coated PLA fibers (designated as Ag/PLA fibers) were obtained. Finally, the Ag/PLA fibers were dispersed in EtOH via vortex mixing (2500 rpm, 10 min), followed by vacuum filtration and hot pressing (120 °C, 10 MPa) to fabricate the Ag/PLA films.

By controlling the alkaline pretreatment time (0, 12, 24, and 36 h), PLA fibers with varying surface roughness were fabricated. To optimize the balance between film thickness and EMI shielding performance, different amounts of Ag/PLA fibers (0.05, 0.1, 0.15, and 0.2 g) were employed. The alkali-treated fibers and their corresponding films are designated as PLA-*x* and Ag/PLA-*x*, respectively, where *x* represents the alkaline pretreatment time in hours. Unless otherwise specified, all samples were prepared using 0.2 g of Ag/PLA fibers subjected to 36 h surface treatment.

2.3 Characterization

The microstructures of the PLA and Ag/PLA fibers were examined using a field emission scanning electron microscope (FESEM, Nova Nano SEM 450, FEI, USA). Prior to observation, all specimens were sputter-coated with a thin layer of platinum to improve imaging

quality. Fiber diameters were quantified from SEM images using ImageJ software. Crystal structure was analyzed via X-ray diffraction (XRD, Rigaku Ultima IV, Japan) employing Cu Kα radiation (λ = 1.5406 Å) over a scanning range of 5°–70° with a step size of 0.02°. Surface wettability was assessed through water contact angle (WCA) on a drop shape analyzer (DSA25, Krüss, Germany). X-ray photoelectron spectroscopy (XPS, K-Alpha, Thermo Scientific, USA) with an Al Kα X-ray source (1486.6 eV) was conducted to determine surface chemical composition and oxidation states. To correct for shifts induced by charge effects, all binding energies were referenced to the C 1s peak at 284.8 eV of surface adventitious carbon. Thermal stability was evaluated by thermogravimetric analysis (TGA, TG 209 F1, NETZSCH, Germany), with samples heated from 30 to 800 °C at a rate of 10 °C/min under nitrogen atmosphere.

The electrical conductivity of the Ag/PLA films was measured using a four-point probe system (RTS-8, Guangzhou Four-Point Probe Technology Co., Ltd., China). A minimum of five specimens per sample group were tested to ensure statistical reliability. The EMI shielding performance of the films was investigated in the X band (8.2–12.4 GHz) using a vector network analyzer (VNA, N5247A, Agilent, USA) equipped with an APC-7 coaxial connector. For this characterization, specimens with a diameter of 13 mm were prepared. The scattering parameters (S-parameters) obtained from the VNA were subsequently utilized to calculate the power coefficients (R, A, and T) and EMI SE values according to the following equations (Eqs. (1)–(6))

$$R = |S_{11}|^2 \tag{1}$$

$$T = |S_{21}|^2 \tag{2}$$

$$A + R + T = 1 \tag{3}$$

$$\mathrm{SE_R} = 10\lg\left(\frac{1}{1-R}\right) \tag{4}$$

$$\mathrm{SE_A} = 10\lg\left(\frac{1-R}{T}\right) \tag{5}$$

$$\mathrm{SE_T} = \mathrm{SE_R} + \mathrm{SE_A} + \mathrm{SE_M} \tag{6}$$

where R, A, and T denote the reflectance, absorptance, and transmittance of electromagnetic waves, respectively. Correspondingly, $\mathrm{SE_R}$ and $\mathrm{SE_A}$ represent the SE attributed to reflection and absorption, respectively. When the total SE ($\mathrm{SE_T}$) exceeds 15 dB, the contribution from multiple reflections ($\mathrm{SE_M}$) can be considered negligible [48].

Furthermore, the specific shielding effectiveness parameters (SE/t and SSE/t), which account for the thickness and density of materials, represent critical metrics for evaluating EMI shielding performance. They are defined as follows (Eqs. (7) and (8))

$$\mathrm{SE}/t = \frac{\text{EMI SE}}{\text{thickness}} \tag{7}$$

$$\mathrm{SSE}/t = \frac{\text{EMI SE}}{\text{density} \times \text{thickness}} \tag{8}$$

3 Results and discussion

3.1 Surface functionalization and electroless Ag plating of PLA fibers

Figure 1(a) schematically illustrates the fabrication process of Ag/PLA fibers, comprising alkaline pretreatment of PLA fibers and subsequent electroless Ag plating. Since the inherently smooth and hydrophobic surface of PLA fibers impedes AgNP deposition, surface treatment prior to electroless plating is essential. The digital photographs reveal the successful transformation from treated PLA fibers (Fig. 1(b)) to Ag/PLA composite fibers with characteristic metallic luster (Fig. 1(c)) after Ag plating.

To elucidate the microstructural evolution induced by alkaline pretreatment, the surface morphology of PLA fibers was examined subjected to various treatment durations (Figs. 1(d)–1(g)). While pristine PLA fibers exhibited smooth and flat surfaces, prolonged alkaline exposure resulted in progressive surface roughening, characterized by increasingly dense and pronounced groove structures (Fig. S1 in the Electronic Supplementary Material (ESM)). Furthermore, statistical analysis of fiber diameter distributions (Fig. S2 in the ESM) demonstrated a systematic reduction correlating with treatment time (Figs. 1(h)–1(k)). This dimensional change can be attributed to the layer-by-layer surface erosion in the low-concentration alkaline solution. The effect was particularly pronounced after 36 h of treatment, with the average fiber diameter decreasing from 14.4 to 6.9 μm.

As depicted in Fig. 2(a), the diffraction peak at 16.8°, corresponding to the (110) crystal plane of PLA, intensifies significantly with prolonged treatment time. Quantitative analysis corroborates this trend, indicating that the crystallinity of the PLA fibers rises from 40.0% to 61.1% after 36 h treatment (Fig. 2(b)). This evolution can be attributed to the preferential alkaline etching of amorphous regions and defective crystalline domains within the semi-crystalline PLA, which effectively increases the crystalline phase fraction.

Moreover, the alkaline pretreatment process hydrolyzes the ester bonds (–COO–) on the PLA surface, introducing hydrophilic carboxyl (–COOH) and hydroxyl (–OH) groups. To visualize the resulting change in wettability, PLA fibers subjected to different treatment durations were dispersed in water (Fig. 2(c)). The untreated (PLA-0) and briefly treated (PLA-12) fibers exhibited pronounced agglomeration and could not be uniformly dispersed. Extending the treatment to 24 h improved dispersion, although slight sedimentation persisted. Notably, the fibers treated for 36 h formed a homogeneous and stable aqueous dispersion, revealing progressive surface hydrophilization. Water contact angle measurements were performed to quantify fiber hydrophilicity (Figs. 2(d) and 2(e)). The pristine PLA fibers demonstrated distinct hydrophobicity with an initial contact angle of 136.0°. As treatment time increased, the water contact angle declined monotonically, reaching 99.2° after 36 h treatment, which approached the hydrophilicity threshold of 90°. Interestingly, within 5 s of droplet deposition on the PLA-36 sample, the contact angle fell to 86.3°, transitioning the surface from hydrophobic to hydrophilic. Upon sustained contact, the angle further decreased to 73.2°. This substantial enhancement in hydrophilicity results from the synergistic effects of increased surface roughness and enriched hydrophilic functional groups on the highly crystalline PLA fiber surfaces.

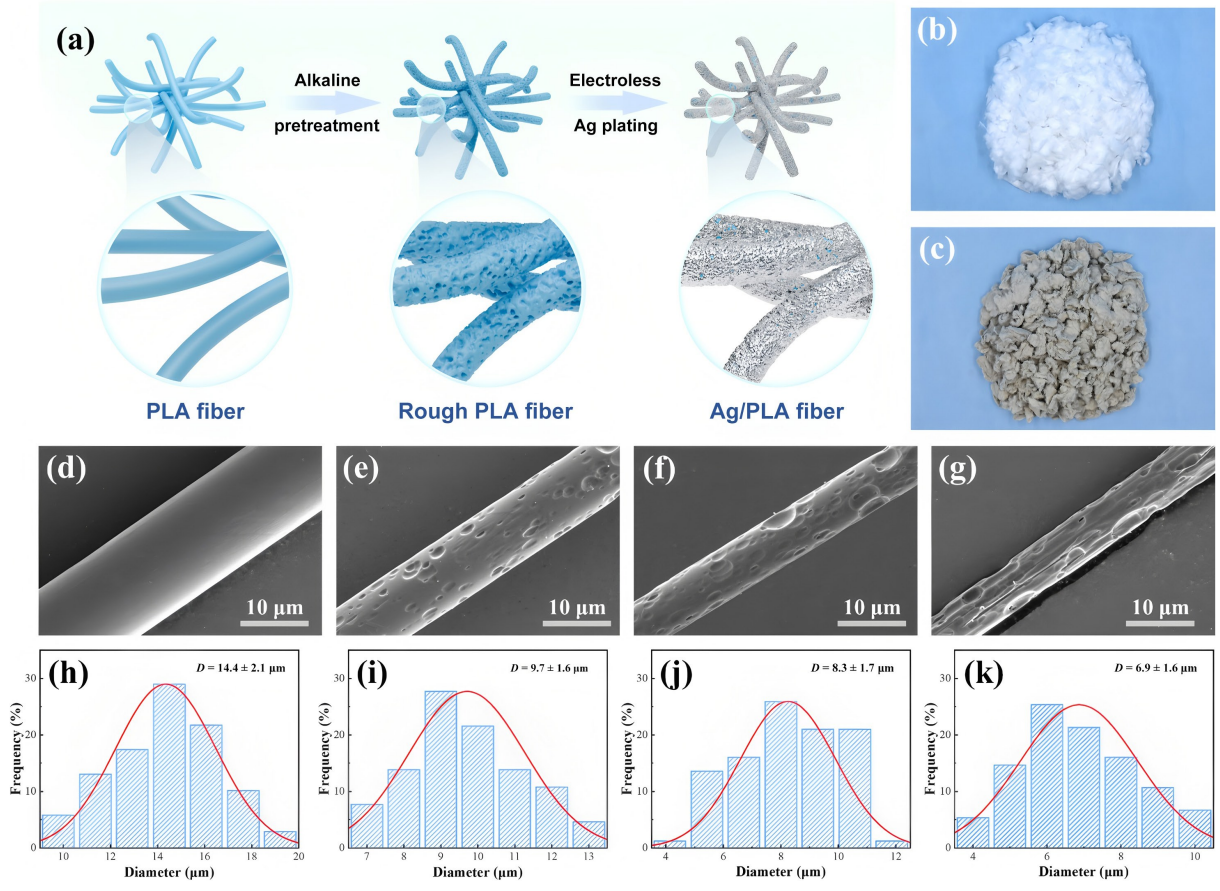

Figure 1 Preparation of Ag/PLA fibers and morphological evolution of PLA fibers under alkaline pretreatment. (a) Schematic illustration of the Ag/PLA fiber fabrication process. Digital photographs of (b) PLA fibers and (c) Ag/PLA fibers. SEM images of PLA fibers after alkaline pretreatment for (d) 0, (e) 12, (f) 24, and (g) 36 h. Corresponding diameter distributions of PLA fibers treated for (h) 0, (i) 12, (j) 24, and (k) 36 h.

To investigate the mechanism underlying the improved hydrophilicity, XPS was employed to characterize the surface chemical composition of representative PLA-0 and PLA-36 fibers. The survey spectra (Fig. 2(f)) exhibited characteristic C 1s and O 1s peaks typical of PLA in both samples. Detailed analysis (Fig. S3 in the ESM) demonstrated that alkaline pretreatment increased the surface oxygen atomic percentage from 33.3% to 36.8%, suggesting the formation of additional oxygen-containing functional groups. High-resolution C 1s spectra of original PLA fibers (Fig. 2(g)) displayed three peaks at 284.8, 287.0, and 289.0 eV, associated with C–C, C–O, and C=O bonds, respectively. Following alkaline pretreatment (Fig. 2(h)), the intensities of C–O and C=O peaks were significantly enhanced. Quantitative deconvolution of the C 1s spectra (Fig. 2(i)) confirmed the increased relative content of these oxygen-containing functional groups, which is consistent with the proposed mechanism of base-catalyzed ester hydrolysis generating carboxyl and hydroxyl groups on the fiber surface.

The influence of alkaline pretreatment duration on subsequent electroless Ag plating was systematically evaluated via morphological characterization of Ag/PLA fiber surfaces (Figs. 3(a)–3(d)). Insufficient pretreatment (0 and 12 h) resulted in sparse and discontinuous AgNP deposition, failing to establish an interconnected conductive network. Extending pretreatment to 24 h substantially improved surface coverage, though minor defects persisted. Complete and uniform AgNP coating was achieved only after 36 h pretreatment (Fig. S4 in the ESM). EDS elemental mapping corroborated these observations, demonstrating a progressive increase in surface AgNP content with prolonged pretreatment duration.

To elucidate the chemical composition and oxidation state of Ag in the optimal Ag/PLA-36 fibers, XPS analysis was performed (Figs. 3(e)–3(i)). The survey spectrum revealed distinct peaks for C 1s, O 1s, and Ag 3d, confirming successful AgNP incorporation. Deconvolution of the high-resolution C 1s spectrum yielded three components at 284.8 (C–C), 286.9 (C–O), and 288.9 eV (C=O), consistent with the PLA molecular structure. The O 1s spectrum exhibited corresponding peaks at 532.2 (C=O) and 533.6 eV (C–O). Notably, the Ag 3d spectrum displayed characteristic spin-orbit splitting with doublet peaks at 368.3 (Ag $3d_{5/2}$) and 374.3 eV (Ag $3d_{3/2}$), accompanied by distinct energy loss features typical of metallic Ag. To definitively rule out the presence of oxidized Ag species, the Ag MNN Auger spectrum was analyzed. The calculated modified Auger parameter (α') of 726.0 eV (Eq. (S1) and Table S1 in the ESM) closely matched the reference value for metallic Ag (~ 726.1 eV), confirming that the AgNPs maintained their metallic state without oxidation.

XRD measurements (Fig. 3(j)) were employed to identify the phase composition of Ag/PLA fibers. The diffraction patterns of Ag/PLA fibers showed four peaks at 16.7°, 38.4°, 44.7°, and 65.0°, assigned to the (110) crystal plane of PLA and the (111), (200), and (220) crystal planes of AgNPs, respectively. As pretreatment duration increased, the PLA diffraction peak gradually diminished while the characteristic AgNP peaks intensified markedly, suggesting enhanced AgNP incorporation within the composite

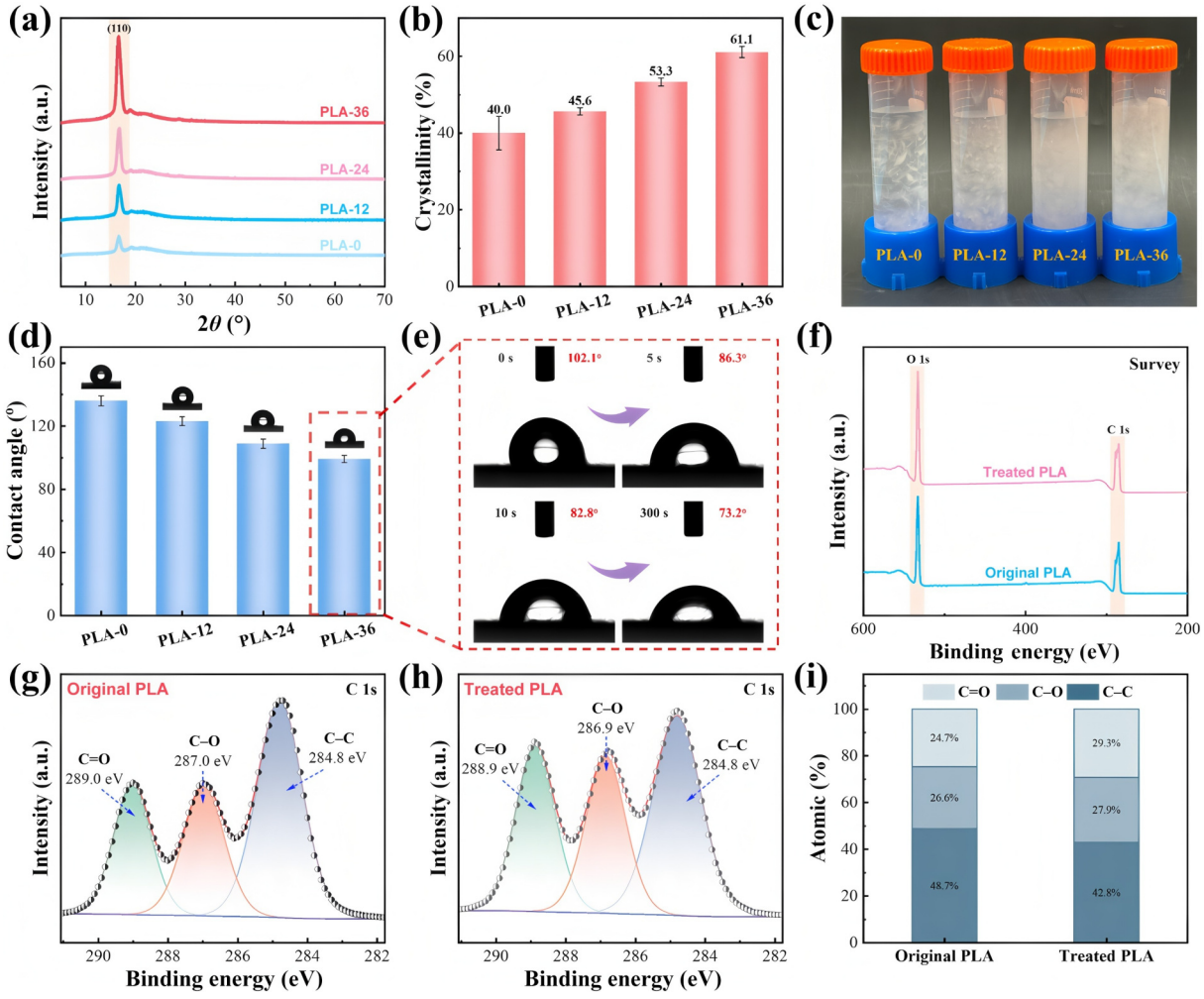

Figure 2 Effects of alkaline pretreatment on the physicochemical properties of PLA fibers. (a) XRD patterns and (b) derived crystallinity of PLA-*x* fibers. (c) Digital photographs of aqueous dispersions of PLA-*x* fibers. (d) Water contact angles of PLA fibers after different pretreatment durations (0, 12, 24, and 36 h), with insets displaying instantaneous contact angle measurements for each sample. (e) Dynamic water contact angle measurements of PLA-36 fibers at 0, 5, 10, and 300 s after droplet deposition. (f) XPS survey spectra of PLA-0 and PLA-36 fibers. High-resolution C 1s spectra of (g) PLA-0 and (h) PLA-36 fibers. (i) Relative contents of surface functional groups (C–C, C=O, and C–O) on PLA fibers before and after alkaline pretreatment.

fibers. To quantify the AgNP loading, TGA was conducted (Figs. 3(k) and 3(l)). Leveraging the differential thermal degradation behaviors of PLA and Ag, the AgNP content was determined using Eqs. S2–S4 in the ESM (detailed in Table S2 in the ESM). The results revealed that extending the treatment time from 0 to 36 h elevated the AgNP content in Ag/PLA fibers from 1.0 vol.% to 9.1 vol.%, with corresponding density rising from 1.3 to 2.1 g/cm^3. Thus, alkaline pretreatment presents an effective strategy for promoting the deposition of AgNPs onto PLA fiber surfaces.

3.2 Electrical and EMI shielding performance of Ag/PLA films

Structuring Ag/PLA fibers into film structures enhances their effectiveness in electrical conductivity and EMI shielding applications. Compared to one-dimensional fibrous structures, two-dimensional films offer significant benefits, including increased effective contact areas and simplified device integration, which greatly expand their practical utility.

The fabrication process of Ag/PLA films is schematically illustrated in Fig. 4(a). The as-prepared Ag/PLA fibers were initially dispersed in EtOH to form a homogeneous suspension, followed by vacuum filtration to induce fiber self-assembly into a free-standing membrane. Subsequently, dense Ag/PLA composite films were obtained via hot-pressing at 120 °C. Notably, the resulting films demonstrated excellent flexibility (Figs. 4(b) and 4(c)), enabling facile transformation into complex three-dimensional architectures such as origami boats and thereby providing a promising platform for flexible electronic applications.

The electrical conductivity of Ag/PLA films (Fig. 4(d)) exhibited a strong positive correlation with the structural integrity of the conductive AgNP layer. The untreated Ag/PLA-0 film displayed a minimal electrical conductivity of 0.0348 S/m, which was attributed to limited AgNP growth on the smooth and hydrophobic surface of pristine PLA fibers. Following pretreatment of 12 and 24 h, the increased surface roughness and hydrophilicity facilitated more effective loading of AgNPs, elevating the electrical conductivity to 650 and 16,520 S/m, respectively. The Ag/PLA-36 film, featuring a dense and continuous AgNP coating on the fiber surface, achieved an electrical conductivity of 102,270 S/m, which was six orders of magnitude higher than the untreated sample.

Furthermore, to demonstrate the practical application potential of Ag/PLA films, a flexible circuit system was constructed (Fig. 4(e)

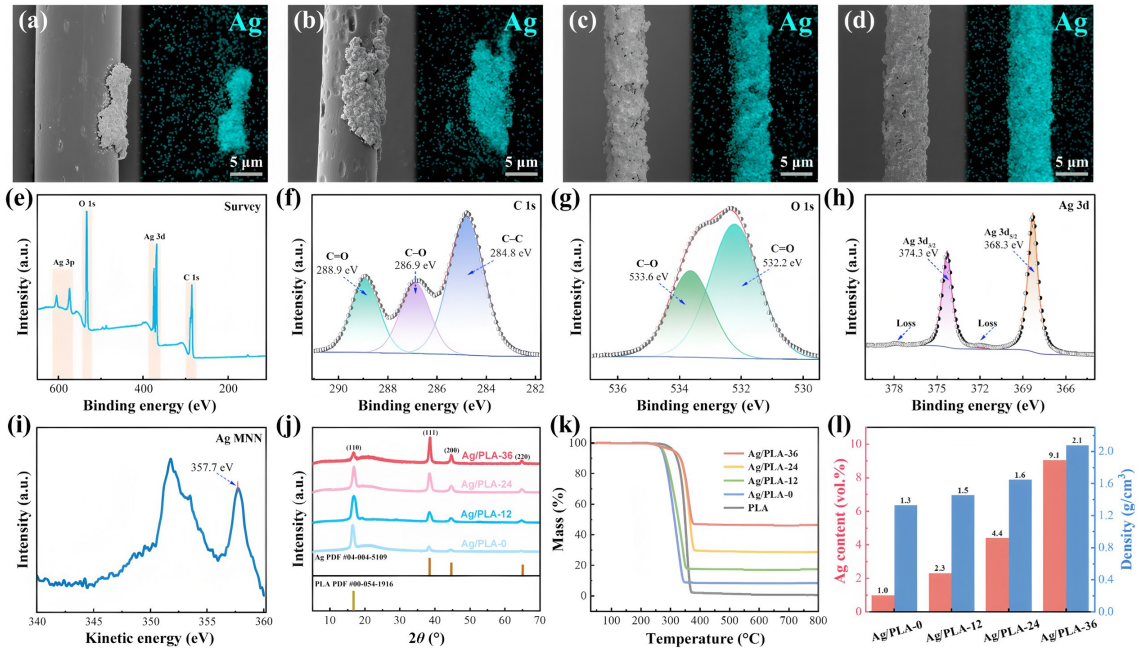

Figure 3 Morphology and chemical composition of Ag/PLA fibers. SEM images and corresponding EDS elemental mapping of Ag/PLA fibers fabricated with alkaline pretreatment for (a) 0, (b) 12, (c) 24, and (d) 36 h. (e) XPS survey spectrum of Ag/PLA-36 fibers. High-resolution XPS spectra of (f) C 1s, (g) O 1s, and (h) Ag 3d regions. (i) Ag MNN Auger spectrum of Ag/PLA-36 fibers. (j) XRD patterns of Ag/PLA-*x* fibers. (k) TGA curves of pristine PLA and Ag/PLA-*x* fibers. (l) Calculated AgNP content and composite fiber density as a function of alkaline pretreatment duration.

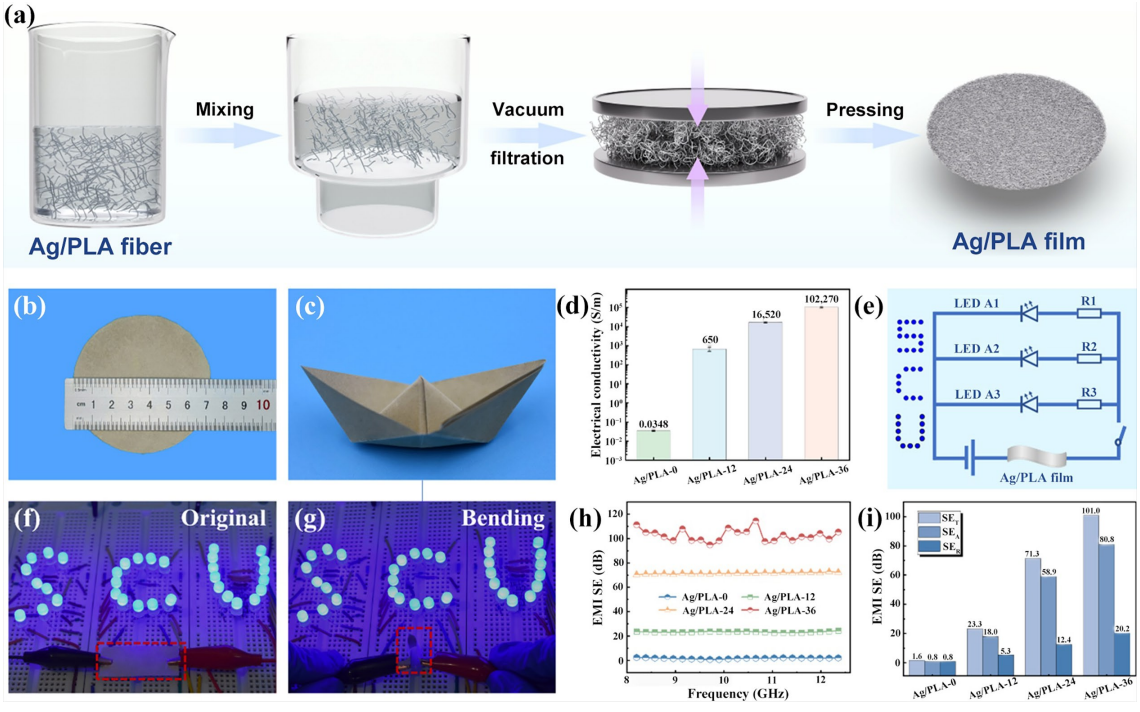

Figure 4 Fabrication, electrical properties, and EMI shielding performance of Ag/PLA films. (a) Schematic illustration of the Ag/PLA film fabrication process. (b) Macroscopic morphology and (c) flexibility demonstration of the Ag/PLA films. (d) Electrical conductivity of Ag/PLA-*x* films. (e) Schematic representation of flexible circuits constructed with Ag/PLA films. Digital photographs demonstrating the electrical conductivity of Ag/PLA films, (f) before and (g) after mechanical bending. (h) EMI SE of Ag/PLA-*x* films in the X-band. (i) Contributions of SE_R and SE_A to the total EMI SE.

and Fig. S5(a) in the ESM). When supplied with direct current, the highly conductive Ag/PLA films successfully illuminated three LED arrays. Remarkably, the LED brightness remained virtually unchanged under various mechanical deformations, including bending, folding, and their combinations (Figs. 4(f) and 4(g), and Figs. S5(b)–5(c) in the ESM). This consistent electrical performance during dynamic deformations validates the structural integrity and robustness of the conductive network within the Ag/PLA films, highlighting their suitability for applications demanding mechanical flexibility, such as flexible displays and wearable electronics.

High electrical conductivity is essential for achieving superior EMI shielding performance. The average EMI SE of Ag/PLA films

in the X-band (8.2–12.4 GHz) increased significantly with prolonged alkaline pretreatment duration (Fig. 4(h)), which aligned with the observed electrical conductivity trends. The untreated Ag/PLA-0 film showed negligible shielding capability (1.6 dB) owing to the absence of an interconnected conductive network. After 12 h of pretreatment, the composite film exhibited an EMI SE of 23.3 dB, exceeding the 20 dB threshold for commercial applications. Importantly, the Ag/PLA-36 film demonstrated exceptional shielding performance with an ultra-high EMI SE of 101.0 dB, attenuating over 99.99999999% of incident electromagnetic waves (EMWs).

To understand the EMI shielding mechanism of Ag/PLA films, the total shielding effectiveness (SE_T) was decomposed into reflection loss (SE_R) and absorption loss (SE_A) components according to Eqs. (1)–(3) (Fig. 4(i)). Both SE_A and SE_R increased with extended pretreatment time, indicating enhanced EMW reflection and absorption capabilities. Specifically, SE_A rose substantially from 0.8 (Ag/PLA-0) to 58.9 dB (Ag/PLA-24), ultimately reaching 80.8 dB (Ag/PLA-36). Correspondingly, SE_R escalated from 0.8 to 12.4 and 20.2 dB following 24 and 36 h pretreatment, respectively. Although SE_A contributed more to SE_T than SE_R across all pretreatment conditions, this observation alone is insufficient to establish an absorption-dominated EMI shielding mechanism. Consequently, power coefficients, including reflectance (R), absorbance (A), and transmittance (T), were analyzed using Eqs. (4)–(6) to determine the primary mechanism (Fig. S6 in the ESM). As the AgNP coating evolved toward greater continuity and completeness, R values climbed from 0.16 to 0.99, whereas A values declined from 0.14 to 0.01. The consistently higher R values relative to A values across all samples confirmed that reflection constitutes the dominant EMI shielding mechanism in Ag/PLA films, which coincides with their high electrical conductivity.

As next-generation electronic devices advance toward miniaturization and high integration, achieving effective EMI shielding with minimal material thickness becomes crucial. To address this challenge, the Ag/PLA-36 films with controlled thicknesses were fabricated by precisely adjusting the amount of composite fibers, and their EMI shielding performance was investigated (Fig. 5(a)). Impressively, the film with a thickness of merely 19 μm exhibited an EMI SE of 38.9 dB, satisfying conventional protection requirements. With increasing thickness to 35 and 50 μm, the average EMI SE reached 63.1 and 81.8 dB, respectively. Furthermore, at a thickness of 66 μm, the Ag/PLA films achieved an ultra-high EMI SE of 101.0 dB, demonstrating superior shielding performance.

To examine the effect of film thickness on the EMI shielding mechanism, SE_A and SE_R were calculated (Fig. 5(b)). At a thickness of 19 μm, the film exhibited SE_A and SE_R values of 24.0 and 14.9 dB,

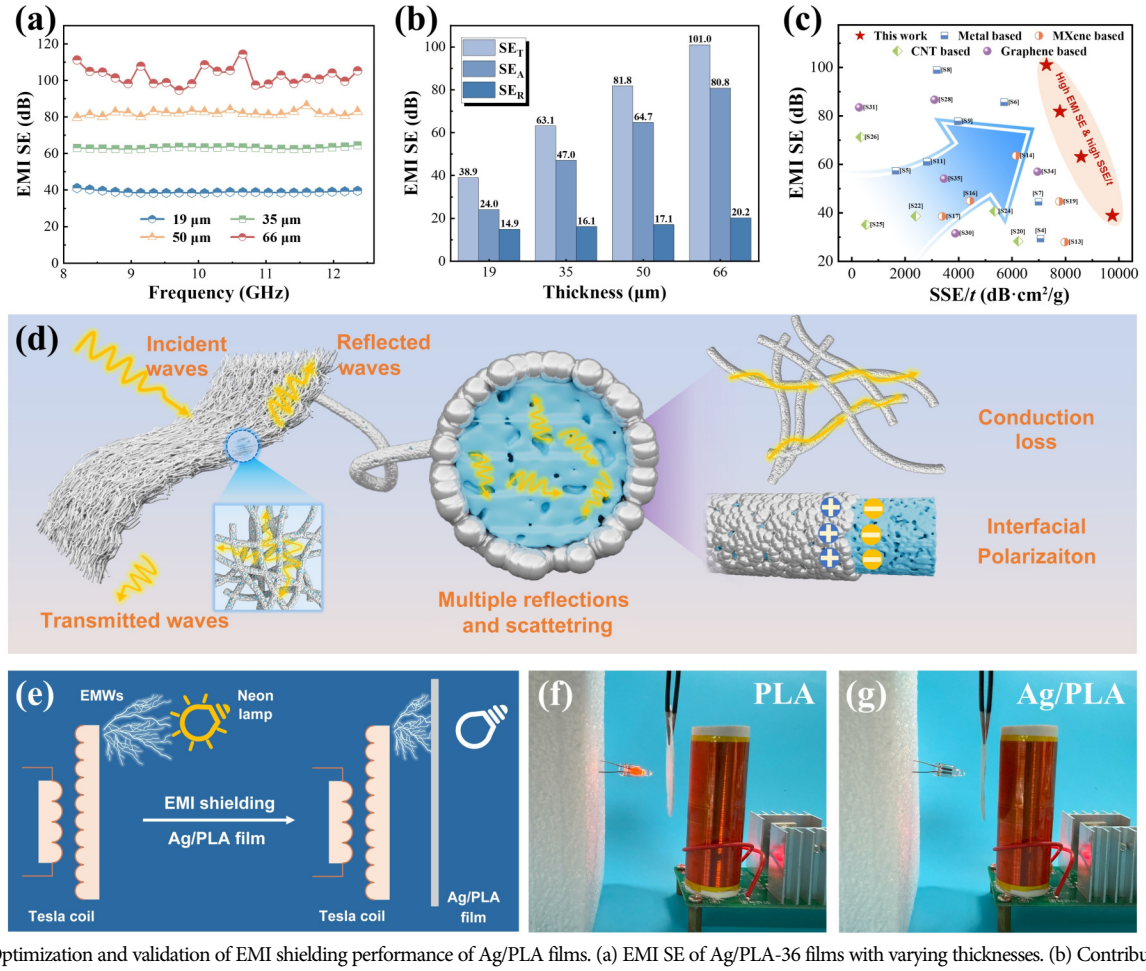

Figure 5 Optimization and validation of EMI shielding performance of Ag/PLA films. (a) EMI SE of Ag/PLA-36 films with varying thicknesses. (b) Contributions of SE_R and SE_A to the total EMI SE. (c) Comparison of the EMI shielding performance of Ag/PLA films with recently reported EMI shielding materials. (d) Schematic illustration of the EMI shielding mechanism in Ag/PLA composite films. (e) Tesla coil experimental setup for shielding visualization. Comparative demonstration of the EMI shielding capability using neon lamp response for (f) pristine PLA film and (g) Ag/PLA film.

respectively, indicating comparable contributions. As thickness increased, SE_A showed a dramatic enhancement, reaching 64.7 dB at 50 μm, whereas SE_R rose only marginally to 17.1 dB. This phenomenon can be attributed to the extended EMW propagation path within thicker films, which facilitated enhanced absorption. In contrast, surface reflection was governed primarily by the intrinsic electrical properties of the material and thus presented minimal thickness dependence. Interestingly, despite the substantially higher SE_A values, power coefficient analysis (Fig. S7 in the ESM) revealed that R values remained consistently high (0.97–0.99) across all thicknesses, while the A values stayed low (0.01–0.03). This apparent contradiction stems from the sequential nature of the shielding process, where reflection occurs before absorption, thereby confirming the reflection-dominant EMI shielding mechanism.

A systematic comparison with other EMI shielding materials reported in the past five years revealed the competitive advantages of the Ag/PLA films. Given the growing demand for lightweight materials in emerging applications, specific shielding effectiveness normalized by thickness (SE/t, Eq. (7)) and density (SSE/t, Eq. (8)) were adopted as primary evaluation metrics (Table S3 in the ESM). The Ag/PLA films exhibited superior SE/t values of 2047.4 dB/mm, significantly surpassing most metal-based, carbon-based, and MXene-based EMI shielding materials (Fig. S8 in the ESM). Remarkably, despite the inherently high density of Ag, the Ag/PLA films achieved an exceptional SSE/t of 9749.4 dB·cm^2/g while maintaining an ultra-high EMI SE of 101.0 dB (Fig. 5(c)). This outstanding comprehensive performance can be attributed to the synergistic integration of the dense and continuous AgNP layer on the fiber surface and the three-dimensional interwoven fibrous architecture, which together establish a highly efficient conductive network.

Based on the aforementioned analysis, the EMI shielding mechanism of Ag/PLA films can be clearly understood (Fig. 5(d)). Upon encountering the film surface, most incident EMWs are immediately reflected due to the pronounced impedance mismatch between free space and the highly conductive AgNP layer. The remaining EMWs that penetrate the film interact with the conductive fibers, inducing currents that dissipate electromagnetic energy into thermal energy via ohmic loss. The core-shell architecture of Ag/PLA composite fibers creates numerous heterogeneous interfaces between the conductive AgNP coating and the insulating PLA matrix. At these interfaces, charge accumulation induces interfacial polarization, thereby enhancing EMW absorption. Furthermore, the inter-fiber gaps and multiple interfaces within the three-dimensional conductive network promote multiple internal reflections and scattering events, providing additional attenuation of electromagnetic radiation. After these shielding mechanisms, EMW transmission through the Ag/PLA film is effectively suppressed, yielding superior EMI shielding performance.

Tesla coils generate high-frequency, high-voltage alternating electromagnetic fields that can wirelessly illuminate neon lamps, providing an ideal platform for visualizing the EMI shielding capability of Ag/PLA films (Fig. 5(e)). When exposed directly to the electromagnetic field or covered with pristine PLA film, the neon lamp remained illuminated (Fig. 5(f) and Fig. S9 in the ESM). However, when shielded with the Ag/PLA composite film (Fig. 5(g)), the lamp extinguished instantly, vividly revealing the successful blocking of electromagnetic field penetration. This demonstration validates the excellent EMI shielding performance of Ag/PLA films and underscores their tremendous potential for protecting sensitive electronic devices from electromagnetic radiation.

3.3 Durability and sustainability of Ag/PLA films

Beyond their prominent EMI shielding performance, the durability of Ag/PLA films in practical applications warrants equal consideration. Novel electronic devices must function reliably across diverse operational environments, encompassing extreme temperatures, corrosive atmospheres, and mechanical degradation. Rigorous assessment of performance stability under such challenging conditions therefore proves indispensable for their successful implementation in real-world applications.

Firstly, the EMI shielding performance of Ag/PLA films was evaluated under extreme temperature conditions. Following exposure to 100 °C for 1 h, the films exhibited an average EMI SE of 97.7 dB, corresponding to 96.3% of the initial value (Fig. 6(a)). Upon cryogenic treatment at liquid nitrogen temperature (−196 °C) for 1 h, the films demonstrated remarkable stability with an EMI SE of 98.9 dB, preserving 97.7% of the original performance (Fig. 6(b)). To analyze thermal cycling stability, the films were subjected to 10 consecutive cycles between 100 and −196 °C, with 1 h dwelling at each temperature extreme (Fig. 6(c)). Despite this severe thermal shock spanning approximately 300 °C, the films still maintained an EMI SE of 92.9 dB (91.4% retention), revealing the exceptional thermomechanical stability of the Ag/PLA films.

High-salt electrochemical corrosion in coastal areas poses a significant challenge for electronic equipment. To examine salt resistance, Ag/PLA films were immersed in a concentrated sodium chloride solution (100 g/L) for 12 h (Fig. 6(d)). The treated films achieved an EMI SE of 98.5 dB, showing only a marginal 2.8% reduction from the initial value. Following 12 months of storage under ambient conditions (25 °C, 70% RH), the films displayed an EMI SE of 95.7 dB (Fig. S10 in the ESM), sustaining 94.9% of the original performance. This excellent durability in both atmospheric and saline environments can be attributed to the intrinsic chemical stability of Ag. Furthermore, the strong adhesion between the AgNP coating and the roughened PLA fiber surface enabled the films to retain an EMI SE of 90.9 dB even after harsh ultrasonic treatment for 1 h (Fig. 6(e)), thereby meeting military-grade specifications (> 90 dB).

Given that flexible EMI shielding materials inevitably undergo mechanical deformation during service, the mechanical robustness of Ag/PLA films was evaluated. Following 5000 bending-releasing cycles (Fig. 6(f)), the films maintained an impressive EMI SE of 93.6 dB, representing only a 7.7% decrease from initial performance. This exceptional mechanical stability originated from the synergistic contribution of the inherent flexibility of the fiber-interwoven network and the robust interfacial adhesion between the AgNP layer and the PLA substrate. Moreover, folding tests (Fig. 6(g)) were performed to validate the durability of Ag/PLA films under more stringent deformation conditions, manifesting an EMI SE of 92.0 dB after multiple folding operations, with 91.0% performance retention. Overall, these results underscore the considerable promise of Ag/PLA films as robust EMI shielding materials for demanding applications in next-generation flexible electronics.

While pursuing high performance, the environmental sustainability of EMI shielding materials has gained increasing attention. Traditional EMI shielding materials, primarily derived

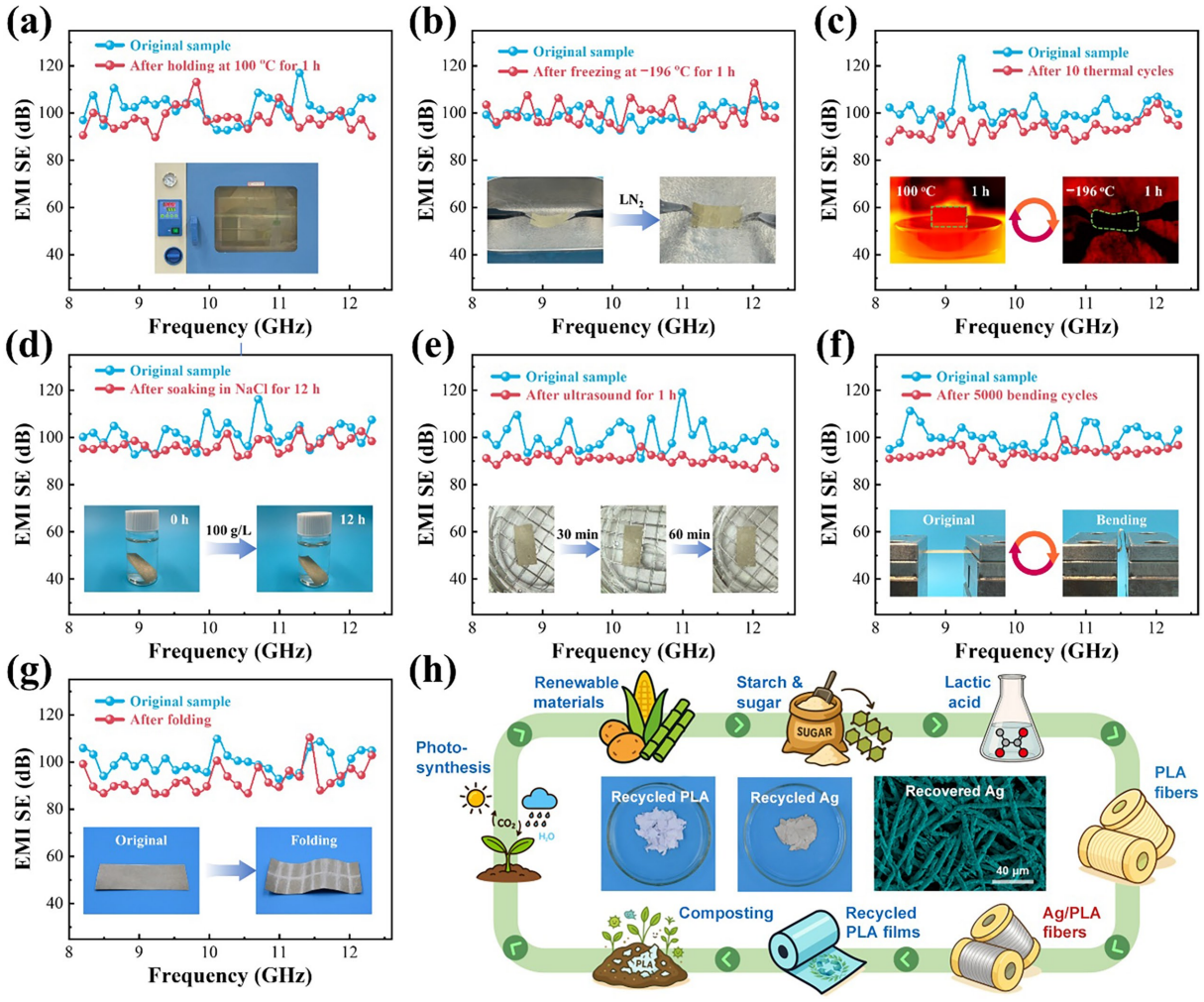

Figure 6 Durability and sustainability assessment of Ag/PLA films. Evolution of EMI SE of Ag/PLA films following (a) high-temperature exposure (100 °C, 1 h), (b) cryogenic exposure (−196 °C, 1 h), (c) 10 thermal cycles, (d) immersion in concentrated saline solution (12 h), and (e) ultrasonication treatment (1 h). EMI shielding performance retention of Ag/PLA films after mechanical deformation through (f) 5000 bending-releasing cycles (bending radius: 1.1 mm) and g) multiple folding operations. (h) Schematic illustration of the closed-loop life cycle for Ag/PLA films. Inset "Recycled PLA" shows a digital photograph of PLA film regenerated *via* dissolution-casting strategy. Insets "Recovered Ag" display (from left to right) a digital photograph and SEM-EDS composite image (Ag shown in blue) of recovered Ag through selective PLA dissolution from the Ag/PLA film.

from petroleum-based polymers, exhibit poor degradability and impose persistent environmental burdens after disposal. In contrast, Ag/PLA films demonstrate comprehensive life-cycle sustainability (Fig. 6(h)). As a bio-based degradable polymer, PLA is sourced from renewable feedstocks such as corn and sugarcane. Specifically, lactic acid obtained through fermentation undergoes polymerization and spinning to produce PLA fibers, which are subsequently processed into Ag/PLA films using the methodology developed in this study. Upon reaching their service life or experiencing unexpected failure, the valuable metal Ag can be fully recovered through selective dissolution of PLA in dichloromethane (Fig. S11 in the ESM). The resulting PLA solution can be reprocessed into films via solvent evaporation, which can then be either reused or subjected to industrial composting. Under composting conditions, PLA undergoes complete degradation into carbon dioxide and water, which serve as nutrients for crop cultivation, thereby establishing a closed-loop "feedstock-product-recovery-regeneration" cycle. This cradle-to-cradle design paradigm not only minimizes resource depletion but also provides a sustainable framework for future EMI shielding materials.

4 Conclusion

In this study, we fabricated Ag/PLA conductive fibers through alkaline pretreatment followed by electroless Ag plating. The alkaline pretreatment selectively etched amorphous regions and defective crystalline domains, significantly enhancing surface roughness while introducing hydrophilic functional groups (carboxyl and hydroxyl) through ester bond hydrolysis. These surface modifications created an optimal substrate for chemical deposition, ensuring both efficient AgNP loading and robust interfacial adhesion. The Ag/PLA fibers were subsequently structured into flexible films via vacuum filtration and hot-pressing, expanding their potential in EMI shielding applications. Benefiting from the dense and continuous AgNP layer on the fiber surface and the three-dimensional interwoven fibrous architecture, the resulting Ag/PLA films demonstrated exceptional electrical conductivity (102,270 S/m), ultra-high EMI SE (101.0 dB), and remarkable SSE/*t* (9749.4 dB·cm²/g). Additionally, the films exhibited excellent durability and mechanical flexibility, maintaining superior EMI SE (> 90 dB with > 90% retention) even after 10 thermal cycles

spanning approximately 300 °C and 5000 bending-releasing cycles. Notably, this material system combines a biodegradable PLA matrix with recoverable precious metal Ag, which offers a sustainable pathway for developing advanced flexible EMI shielding materials that meet the stringent requirements of next-generation electronic devices.

Electronic Supplementary Material: Supplementary Material (pore size distribution, relative elemental content, AgNP content, power coefficient calculations, comprehensive comparison with other EMI shielding materials, and long-term stability assessment of EMI shielding performance) is available in the online version of this article at https://doi.org/10.26599/NR.2026.94908333.

Data availability

All data needed to support the conclusions in the paper are presented in the manuscript and the Electronic Supplementary Material. Additional data related to this paper may be requested from the corresponding author upon request.

Acknowledgements

The authors gratefully acknowledge financial support from the National Natural Science Foundation of China (Nos. U24A2074, 52403045, 52473044, and 52273270), the Postdoctoral Fellowship Program of CPSF (No. GZC20241106), the Opening Project of Robotic Satellite Key Laboratory of Sichuan Province, and the Sichuan University Postdoctoral Interdisciplinary Innovation Fund.

Declaration of competing interest

All the contributing authors report no conflict of interests in this work.

Author contribution statement

J.-L. Z.: Methodology, investigation, formal analysis, writing – original draft. S. Y.: Investigation, formal analysis, visualization. J. L.: Conceptualization, methodology, supervision, writing – review & editing. Y.-Y. W.: Writing – review & editing. L. X.: Resources. G.-J. Z.: Resources. D.-X. Y.: Conceptualization, funding acquisition, writing – review & editing. Z.-M. L.: Funding acquisition, project administration.

Use of AI statement

None.

References

[1] He, M. K.; Hu, J. W.; Yan, H.; Zhong, X.; Zhang, Y. L.; Liu, P. B.; Kong, J.; Gu, J. W. Shape anisotropic chain-like CoNi/polydimethylsiloxane composite films with excellent low-frequency microwave absorption and high thermal conductivity. *Adv. Funct. Mater.* **2025**, *35*, 2316691.

[2] Isari, A. A.; Ghaffarkhah, A.; Hashemi, S. A.; Wuttke, S.; Arjmand, M. Structural design for EMI shielding: From underlying mechanisms to common pitfalls. *Adv. Mater.* **2024**, *36*, 2310683.

[3] Liu, A.; Qiu, H.; Lu, X. H.; Guo, H.; Hu, J. W.; Liang, C. B.; He, M. K.; Yu, Z.; Zhang, Y. L.; Kong, J. et al. Asymmetric structural MXene/PBO aerogels for high-performance electromagnetic interference shielding with ultra-low reflection. *Adv. Mater.* **2025**, *37*, 2414085.

[4] Yang, Y. F.; Li, B.; Wu, N.; Liu, W.; Zhao, S. Y.; Zhang, C. J.; Liu, J. R.; Zeng, Z. H. Biomimetic porous MXene-based hydrogel for high-performance and multifunctional electromagnetic interference shielding. *ACS Mater. Lett.* **2022**, *4*, 2352–2361.

[5] Liu, M.; Chen, K. X.; Shi, Y. Q.; Wang, H. R.; Wu, S. J.; Huang, R. Z.; Feng, Y. Z.; Tang, L. C.; Liu, X. H.; Song, P. A. High-performance flexible nanocomposites with superior fire safety and ultra-efficient electromagnetic interference shielding. *J. Mater. Sci. Technol.* **2023**, *166*, 133–144.

[6] Zhang, Y. L.; Gu, J. W. A perspective for developing polymer-based electromagnetic interference shielding composites. *Nano-Micro Lett.* **2022**, *14*, 89.

[7] Issman, L.; Alper, M.; Howard, S.; Karch, C.; Yeshurun, S.; Pick, M.; Boies, A. Direct-spun CNT textiles for high-performance electromagnetic interference shielding in an ultra-wide bandwidth. *Carbon* **2023**, *206*, 166–180.

[8] Cui, Z. R.; Yang, M. L.; Han, G. Y.; Zhang, H.; Wang, Y.; Zhang, Y.; Li, Z. Y.; He, J. Z.; Yu, R. H.; Shui, J. L. et al. Recent advances in carbon composite films for high-performance, multifunctional and intelligent electromagnetic interference shielding and electromagnetic wave absorption. *Carbon* **2024**, *230*, 119627.

[9] Wang, M.; Tang, X. H.; Cai, J. H.; Wu, H.; Shen, J. B.; Guo, S. Y. Construction, mechanism and prospective of conductive polymer composites with multiple interfaces for electromagnetic interference shielding: A review. *Carbon* **2021**, *177*, 377–402.

[10] Li, Z. Y.; Zhang, F.; Zong, Z.; Liu, M. X.; Xu, H. K.; Deng, Z. H.; Wang, Y. Y.; Yan, D. X.; Li, Z. M. Flexible aramid fiber-based film with hollow microsphere structure for efficient microwave absorption. *J. Mater. Sci. Technol.* **2026**, *253*, 289–297.

[11] Zhang, Y. L.; Liu, A.; Tian, Y. Y.; Tian, Y. J.; Qi, X. S.; Qiu, H.; He, M. K.; Zhou, K.; Gu, J. W. Direct-ink-writing printed aerogels with dynamically reversible thermal management and tunable electromagnetic interference shielding. *Adv. Mater.* **2025**, *37*, 2505521.

[12] Wang, Y. Y.; Yang, S.; Sun, W. J.; Dai, K.; Yan, D. X.; Li, Z. M. Highly enhanced microwave absorption for carbon nanotube/barium ferrite composite with ultra-low carbon nanotube loading. *J. Mater. Sci. Technol.* **2022**, *102*, 115–122.

[13] Zhai, M. Z.; Zhao, S. J.; Guo, H.; Li, X. C.; Shi, X. T.; He, M. K.; Zhang, Y. L.; Gu, J. W. Bionic-structured electromagnetic interference shielding composites. *Sci. Bull.* **2025**, *70*, 2347–2364.

[14] Li, J.; Zhang, J. L.; Yong, S.; Zhong, G. J.; Lei, J.; Wang, Y. Y.; Xu, L.; Yan, D. X.; Li, Z. M. Stable and elastic electromagnetic interference shielding composites with microtubule-like silver nanoparticles via swelling-dissolution strategy. *Small* **2025**, *21*, e07054.

[15] Li, P.; Wang, H. N.; Ju, Z. S.; Jin, Z. Z.; Ma, J. G.; Yang, L.; Zhao, X. N.; Xu, H. Y.; Liu, Y. C. $Ti_3C_2T_x$ MXene- and sulfuric acid-treated double-network hydrogel with ultralow conductive filler content for stretchable electromagnetic interference shielding. *ACS Nano* **2024**, *18*, 2906–2916.

[16] Zhao, H.; Wang, J. F.; He, M. K.; Li, S.; Guo, H.; Kan, D. X.; Qiu, H.; Chen, L. X.; Gu, J. W. Electromagnetic interference shielding films: Structure design and prospects. *Small Methods* **2025**, *9*, 2401324.

[17] Zhao, G. J.; Cao, X. Y.; Zhang, Q.; Deng, H.; Fu, Q. A novel interpenetrating segregated functional filler network structure for ultra-high electrical conductivity and efficient EMI shielding in CPCs containing carbon nanotubes. *Mater. Today Phys.* **2021**, *21*, 100483.

[18] Kim, J.; Kim, G.; Kim, S. Y.; Lee, S.; Kim, Y.; Lee, J.; Kim, J.; Jung, Y. C.; Kwon, J.; Han, H. Fabrication of highly flexible electromagnetic interference shielding polyimide carbon black composite using hot-pressing method. *Compos. B: Eng.* **2021**, *221*, 109010.

[19] Zhang, Y. L.; Ruan, K. P.; Gu, J. W. Flexible sandwich - structured electromagnetic interference shielding nanocomposite films with

excellent thermal conductivities. *Small* **2021**, *17*, 2101951.
[20] Ma, R. Y.; Yi, S. Q.; Li, J.; Zhang, J. L.; Sun, W. J.; Jia, L. C.; Yan, D. X.; Li, Z. M. Highly efficient electromagnetic interference shielding and superior mechanical performance of carbon nanotube/polydimethylsiloxane composite with interface-reinforced segregated structure. *Compos. Sci. Technol.* **2023**, *232*, 109874.
[21] Liu, L. X.; Chen, W.; Zhang, H. B.; Wang, Q. W.; Guan, F. L.; Yu, Z. Z. Flexible and multifunctional silk textiles with biomimetic leaf‐like MXene/silver nanowire nanostructures for electromagnetic interference shielding, humidity monitoring, and self‐derived hydrophobicity. *Adv. Funct. Mater.* **2019**, *29*, 1905197.
[22] Zhang, Y. L.; Ruan, K. P.; Zhou, K.; Gu, J. W. Controlled distributed $Ti_3C_2T_x$ hollow microspheres on thermally conductive polyimide composite films for excellent electromagnetic interference shielding. *Adv. Mater.* **2023**, *35*, 2211642.
[23] Yang, B.; Wang, H. R.; Zhang, M. Y.; Jia, F. F.; Liu, Y. Q.; Lu, Z. Q. Mechanically strong, flexible, and flame-retardant $Ti_3C_2T_x$ MXene-coated aramid paper with superior electromagnetic interference shielding and electrical heating performance. *Chem. Eng. J.* **2023**, *476*, 146834.
[24] Wu, L. P.; Li, Y. Z.; Wang, B. J.; Mao, Z. P.; Xu, H.; Zhong, Y.; Zhang, L. P.; Sui, X. F. Electroless Ag-plated sponges by tunable deposition onto cellulose-derived templates for ultra-high electromagnetic interference shielding. *Mater. Des.* **2018**, *159*, 47–56.
[25] Muench, F. Electroless plating of metal nanomaterials. *ChemElectroChem* **2021**, *8*, 2993–3012.
[26] Kim, N. K.; Kang, S. M.; Kim, T.; Kim, S.; Kim, G. H. Electroless plating on polymer surfaces: Comprehensive review of mechanism, process, analysis, and future applications. *Adv. Mater. Interfaces* **2025**, *12*, 2400931.
[27] Yang, G.; Wang, M. J.; Dong, J. W.; Su, F. M.; Ji, Y. X.; Liu, C. T.; Shen, C. Y. Fibers-induced segregated-like structure for polymer composites achieving excellent thermal conductivity and electromagnetic interference shielding efficiency. *Compos. B: Eng.* **2022**, *246*, 110253.
[28] Deng, L. C.; Yang, K.; Wang, W. Z.; Zhang, W. J.; Li, Y.; Nan, H. Y.; Chai, X.; Luo, F.; Wu, H. J.; Chen, Q. Ag-doped PDA interface strategy for selective electron transition integrating EMI shielding and anti-corrosion performance. *J. Mater. Sci. Technol.* **2025**, *224*, 292–301.
[29] Zhang, J. L.; Yong, S.; Wang, T.; Feng, J.; Li, J.; Wang, Y. Y.; Xu, L.; Zhong, G. J.; Lei, J.; Yan, D. X. et al. Flexible and ultra-high electromagnetic interference shielding films with fiber-bridged segregated conductive network. *Chem. Eng. J.* **2025**, *519*, 165305.
[30] Li, J.; Luo, K. C.; Zhang, J. L.; Lei, J.; Lin, H.; Tang, J. H.; Zhong, G. J.; Yan, D. X.; Li, Z. M. Flexible and water-proof nylon mesh with ultralow silver content for effective electromagnetic interference shielding effectiveness. *Chem. Eng. J.* **2022**, *439*, 135662.
[31] Xiao, R. M.; Yu, G. Q.; Xu, B. B.; Wang, N.; Liu, X. Q. Fiber surface/interfacial engineering on wearable electronics. *Small* **2021**, *17*, 2102903.
[32] Zhou, S. X.; Dong, J.; Li, X. T.; Zhao, X.; Zhang, Q. H. Continuous surface metallization of polyimide fibers for textile-substrate electromagnetic shielding applications. *Adv. Fiber Mater.* **2023**, *5*, 1892–1904.
[33] Zhang, T. Y.; Guo, J. L.; Liu, S. J.; Gong, L.; Hao, X. Y.; Ye, Q.; Kang, J. Y.; Cao, L.; Liu, X. Q. Enhanced electroless metallization of aramid fibers *via* non-destructive π-π surface engineering for EMI shielding. *Compos. Sci. Technol.* **2025**, *269*, 111236.
[34] Xu, Y.; Li, Y.; Hua, W.; Zhang, A. M.; Bao, J. J. Light-weight silver plating foam and carbon nanotube hybridized epoxy composite foams with exceptional conductivity and electromagnetic shielding property. *ACS Appl. Mater. Interfaces* **2016**, *8*, 24131–24142.
[35] Ren, W.; Yang, Y. Q.; Yang, J.; Duan, H. J.; Zhao, G. Z.; Liu, Y. Q. Multifunctional and corrosion resistant poly(phenylene sulfide)/Ag composites for electromagnetic interference shielding. *Chem. Eng. J.* **2021**, *415*, 129052.
[36] Tang, X. W.; Lu, Y. Z.; Li, S. S.; Zhu, M. Y.; Wang, Z. X.; Li, Y.; Hu, Z. Y.; Zheng, P. L.; Wang, Z. C.; Liu, T. X. Hierarchical polyimide nonwoven fabric with ultralow-reflectivity electromagnetic interference shielding and high-temperature resistant infrared stealth performance. *Nano-Micro Lett.* **2025**, *17*, 82.
[37] Oh, K. W.; Kim, D. J.; Kim, S. H. Improved adhesion property and electromagnetic interference shielding effectiveness of electroless Cu‐plated layer on poly(ethylene terephthalate) by plasma treatment. *J. Appl. Polym. Sci.* **2002**, *84*, 1369–1379.
[38] Zeng, Z. H.; Jiang, F. Z.; Yue, Y.; Han, D. X.; Lin, L. C.; Zhao, S. Y.; Zhao, Y. B.; Pan, Z. Y.; Li, C. J.; Nyström, G. et al. Flexible and ultrathin waterproof cellular membranes based on high-conjunction metal-wrapped polymer nanofibers for electromagnetic interference shielding. *Adv. Mater.* **2020**, *32*, 1908496.
[39] Qiu, Q.; Guo, Y. B.; Sun, Q.; Lu, Y. X. Studies on preparation and reversed electromagnetic interference shielding behavior from GHz to THz of multifunctional wearable Ni/CP composite. *Chem. Eng. J.* **2025**, *503*, 158224.
[40] Gupta, B.; Revagade, N.; Hilborn, J. Poly(lactic acid) fiber: An overview. *Prog. Polym. Sci.* **2007**, *32*, 455–482.
[41] Zhang, Q.; Wang, K.; Chen, X. C.; Tang, X. H.; Zhao, Q.; Fu, Q. Biomass composite based on metallized bamboo fiber for electromagnetic interference shielding, joule heating, and solar heating. *Compos. Sci. Technol.* **2023**, *243*, 110228.
[42] Xie, H. H.; Lu, Y.; Zhao, X. L.; Zeng, J. B.; Wang, M.; Li, Y. D. Ultrahigh strength poly(lactic acid) composites with superior EMI shielding performance enabled by synergistic effect of short carbon fibers and carbon nanotubes. *Compos. Sci. Technol.* **2025**, *261*, 111045.
[43] Rasal, R. M.; Janorkar, A. V.; Hirt, D. E. Poly(lactic acid) modifications. *Prog. Polym. Sci.* **2010**, *35*, 338–356.
[44] Sun, S. P.; Wei, M.; Olson, J. R.; Shaw, M. T. Alkali etching of a poly(lactide) fiber. *ACS Appl. Mater. Interfaces* **2009**, *1*, 1572–1578.
[45] Yang, J.; Wan, Y. Q.; Tu, C. F.; Cai, Q.; Bei, J. Z.; Wang, S. G. Enhancing the cell affinity of macroporous poly(L-lactide) cell scaffold by a convenient surface modification method. *Polym. Int.* **2003**, *52*, 1892–1899.
[46] Karamanlioglu, M.; Robson, G. D. The influence of biotic and abiotic factors on the rate of degradation of poly(lactic) acid (PLA) coupons buried in compost and soil. *Polym. Degrad. Stab.* **2013**, *98*, 2063–2071.
[47] Luzi, F.; Fortunati, E.; Puglia, D.; Petrucci, R.; Kenny, J. M.; Torre, L. Study of disintegrability in compost and enzymatic degradation of PLA and PLA nanocomposites reinforced with cellulose nanocrystals extracted from *Posidonia Oceanica*. *Polym. Degrad. Stab.* **2015**, *121*, 105–115.
[48] Liu, A.; Xu, X. S.; Qiu, H.; Guo, H.; He, M. K.; Yu, Z.; Zhang, Y. L.; Gu, J. W. Bioinspired hollow heterostructure fillers for enhanced electromagnetic interference shielding in polyimide aerogels. *InfoMat* **2025**, *7*, e70060.